Voltammetric Characterization of DNA Intercalators across the Full pH Range: Anthraquinone-2,6-disulfonate and Anthraquinone-2-sulfonate

Christopher Batchelor-McAuley, Qian Li, Sophie M. Dapin, and Richard G. Compton*

Department of Chemistry, Physical and Theoretical Chemistry Laboratory, Oxford University, South Parks Road, Oxford OX1 3QZ, United Kingdom

Received: January 27, 2010; Revised Manuscript Received: February 12, 2010

The use of anthraquinone and its derivatives, notably the sulfonate and disulfonate salts, for the detection of DNA via electrochemical techniques, has been the focus of a number of recent articles. This study provides a quantitative model of the two redox systems of anthraquinone-2,6-disulfonate and anthraquinone-2-sulfonate, over the full aqueous pH range (0−13); the model is based upon the theoretical "scheme of squares" for a $2H^+$, $2e^-$ system, as first proposed by Jacq (Jacq, J. *J. Electroanal. Chem.* **1971**, *29*, 149−180). The effect of pH and ionic strength on the observed cyclic voltammetry was investigated experimentally. The variation of the electrochemical response with proton concentration was modeled through use of the commercially available simulation software, DIGISIM; the system was successfully fitted with attention to voltammetric peak height, position, width, and shape. The model demonstrates how the pK_a values of the anthraquinone intermediates dominate the observed pH dependence of the voltammetry. At high pH (above pH 12), a simple EE process is found to occur. As the pH decreases, the formation of other protonated species becomes possible; this not only causes a Nernstian shift in the measured electrochemical potential for the redox couple but also results in changes in the mechanistic pathway. At pH 10, an EECC process dominates, as the pH is further lowered into the range 4−7, the overall mechanism is an ECEC process, and finally a CECE mechanism opperates at around pH 1 and below. This work provides physical insight into the complex mechanistic pathways involved and will aid the future development of more sophisticated and accurate anthraquinone based DNA sensors.

Introduction

A widespread strategy for electrochemical DNA detection is the utlization of a label, which binds to DNA. While metal nanoparticles[2] and enzymes[3−5] have been used in this context, the most commonly adopted label is that of a redox active molecule, especially ones which either intercalate between two adjacent base pairs or else interact with the DNA major or minor groove.[6] For intercalation, flat, planar molecules are appropriate and examples include methylene blue[7] and metal complexes,[8] although the approach is perhaps best developed through the use of anthraquinone derivatives,[9] including work where anthraquinone has been specifically modified for the purpose of being a DNA hybridization indicator.[10] Some of the analyses simply involve addition of the reagent to the solution containing DNA, which has the considerable advantage that prior labeling of reagents is unnecessary and the method is therefore "universal" in nature.[11]

Double stranded DNA has been shown to transfer charge through it base pairs[12] over distances of up to 35 Å; furthermore, this property is also known to be influenced by the presence of base pair mismatches.[13] Among others, Wong and Gooding[14] utilized this charge transfer ability to produce a sequence specific DNA sensor, whereby anthraquinone-2,6-disulfonic acid (2,6-AQDS) acted as a redox probe where the reductive redox signal decreased in the presence of C−A or G−A base pair mismatches. This methodology was further developed to allow in situ testing using anthraquinone-2-sulfonic acid (2-AQMS), this is possible due to the observed shift in electrochemical potential for the DNA bound form of the intercalator.[9,15] Work done with the intercalation of anthraquinone derivatives into DNA has generally been undertaken in buffered media at around neutral pH. At these levels of proton concentration, the reduction of the AQ derivative will result in the formation of the fully protonated form (due to the associated pK_a values) and will likely follow a complex mechanistic pathway, involving the monoprotonated semiquinone radical.

The use of anthraquinone (AQ) derivatives, notably the sulfonate and disulfonate salts, is necessitated due to the low water solubility of the underivatized form, viz., anthraquinone itself (6.5 μmol dm^{-3}).[16] The chemical structures of 2,6-AQDS and 2-AQMS are shown in Figure 1. Under buffered acidic conditions and sufficiently driving negative potentials, the reduction of AQ or its derivatives proceeds via a two-electron, two-proton process:

$$AQ + 2H^+ + 2e^- \rightleftharpoons AQH_2 \qquad (1)$$

However, under other conditions (i.e., in nonaqueous media or solutions of differing pH), the process can, at least in principle, stop at a lower protonated or electronic state. Moreover, even if the process is overall a two-electron, two-proton system, the precise mechanism, i.e., the sequence of the addition of electrons and protons, can be pH dependent. Accordingly, the voltammetric signals seen for reaction 1 can be expected to and in fact do vary considerably with pH. Furthermore, there is evidence that, with the case of sulfonated anthraquinones, these molecules can interact with cations present in solution.[17,18]

* Corresponding author. Fax: +44 (0) 1865 275410. Phone: +44 (0) 1865 275413. E-mail: richard.compton@chem.ox.ac.uk.

10.1021/jp1008187
Published on Web 03/02/2010

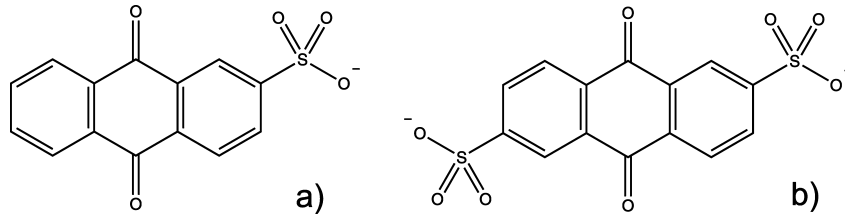

Figure 1. The structures of (a) anthraquinone-2-sulfonate (2-AQMS) and (b) anthraquinone-2,6-disulfonate (2,6-AQDS).

Accordingly, it follows that the use of reaction 1 as a voltammetric probe is highly medium (solvent and electrolyte) dependent.

In the present paper, we investigate the quantitative characteristics of the redox of anthraquinone-2,6-disulfonic acid and anthraquinone-2-sulfonic acid over the full pH range and in the presence of variable amounts of Na^+ and K^+ ions. The variation in the peak potential and current is shown to vary significantly and has been successfully modeled, to describe the mechanistic rates, as a function of pH ($0 < pH < 13$). We believe this quantified model provides an excellent platform on which the construction of anthraquinone based biosensors can be initiated. Moreover, from a physical electrochemical perspective, we believe these studies to be the first case of a "scheme of squares" analysis of a $2H^+$, $2e^-$ reaction over a full pH range of pH 0−13. As the proton concentration is varied, the electrochemical reduction mechanism is shown to change from a simple EE process at high pH. Then, as the pH is lowered to around 10, an EECC mechanism predominately operates, at lower pH (4−7) an ECEC process occurs, and finally at low pH (around pH 1) the reduction follows a CECE type mechanism. The change in mechanism is a result of various protonated intermediates becoming involved in the electrochemical reaction as the pH is lowered; this is due to their associated acid dissociation constants.

Experimental Methods

All reagents were purchased from Aldrich (Gillingham, U.K.) and were used as received without further purification. All solutions were prepared using deionized water of resistivity not less than 18.2 MΩ cm at 298 K (Viviendi water systems, U.K.). Electrochemical measurements were recorded using a computer controlled μAutolab potentiostat (EcoChemie) with a standard three-electrode configuration in a buffered solution. The following buffers were used: pH 0−2 (HCl, 0.1 M KCl), pH 3 (0.1 M citric acid, 0.1 M KCl), pH 4−5 (50 mM acetic acid, 50 mM sodium acetate, 0.1 M KCl), pH 6−8 (50 mM monobasic potassium phosphate, 50 mM dibasic potassium phosphate, 0.1 M KCl), pH 9−10 (0.1 M disodium tetraborate, 0.1 M KCl), pH 11 (50 mM phenol, 50 mM phenoxide, 0.1 M KCl), and pH 12−13 (NaOH, 0.1 M KCl). Concentrated NaOH or HCl was used to adjust the pH to the desired level. The pH of the solution was measured using a pH213 Microprocessor pH meter (Hanna Instruments, Leighton Buzzard, U.K.). A polycrystalline gold working electrode was used, of diameter 1.6 mm (BASi Technicol, West Lafayette, IN) or 25 μm (Cypress Systems Ltd., Chelmsford, MA). A platinum wire (99.99% GoodFellow, Cambridge, U.K.) counter electrode and a saturated calomel reference electrode (SCE, Radiometer, Copenhagen, Denmark) completed the cell assembly. The Au electrodes were polished using alumina slurries of decreasing size from 3.0 to 0.1 μm (Buehler Micropolishing II, Lake Bluff, IL) with the electrode briefly sonicated between each polishing step to remove any adhered alumina microparticles. All experiments were carried out at 20 ± 2 °C.

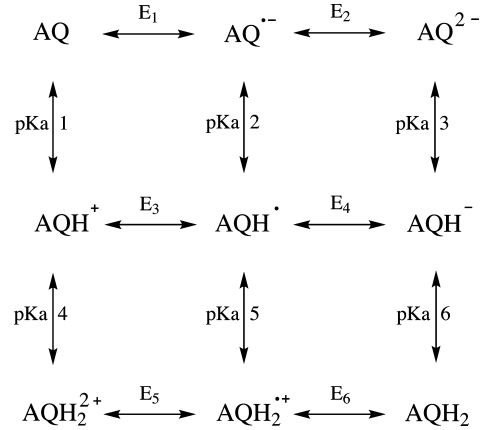

Figure 2. Generalized "scheme of squares" for the anthraquinone $2H^+$, $2e^-$ redox system.

Theory

Due to quinones being present in a number of biological systems, their electrochemical properties have long been studied. A theoretical description of the $2H^+$, $2e^-$ system was first proposed by Jacq,[1] this "scheme of squares" model is based upon the assumption that electron transfer is the rate limiting step and the protonations are at equilibrium. A generalized scheme for the anthraqinone redox system is presented in Figure 2. The mechanistic pathway taken is heavily dependent upon the associated pK_a values of the intermediate species and the pH of the local environment. Jacq's work was later developed by Laviron[19] where it was demonstrated that, where the transfer coefficient (α) is 0.5 and all diffusion coefficients are equal, this scheme behaves as a simple reaction with two successive one-electron transfers, with apparent rate constants and standard potentials. This has been applied to the analysis of the kinetics of *p*-benzoquinone reduction on a platinum electrode.[20] A complete scheme of squares has been approximately *calculated* for 2,6-AQDS by Rosso et al.[21] by conversion of electron affinities in the gas phase to reduction potentials, but the values obtained are not realistic for media involving hydrogen bonding. The calculated potentials for first and second electron transfer differ by 107 mV; in such a case at high pH, two consecutive one-electron transfers would be observed, as per aprotic media; experimentally in aqueous media, one peak is observed.

The electrochemical response of quinones differs greatly between protic and aprotic media, in which they tend to show one and two electron waves, respectively. This incongruous behavior was explained by Quan et al.[22] whom demonstrated the role of hydrogen bonding in stabilizing the reduced dianion form of the quinone. Recent work has also aimed to apply the "scheme of squares" to the simulation and analysis of the redox behavior of flavin adenine dinucleotide, but this work was only focused on a limited pH range (5−9). This analysis did not involve the use of the diprotonated oxidized or the unprotonated reduced forms; pK_a values were specifically chosen so that they did not contribute to the overall observed current. Furthermore,

the simulation is simplified by the assumption that all electron transfer rate constants are arbitrarily high with a value of 10^4 cm s^{-1} being used universally. Comparison of this work to experimental data was exclusively limited to the position of the peak potential of the reductive wave[23,24] and ignored the magnitude of the voltammetric waves, their shapes, and their peak to peak widths. Work by Henstridge et al.[25] has also utilized DIGISIM to simulate solution phase 2-AQMS, demonstrating that the full "scheme of squares" can be used to provide a system in which the simulated voltammetry varies with 59 mV/pH. The pK_a values used in this work do not mirror those found within the literature; furthermore, no comparison with experimental data is provided.

Results

Diffusion Coefficient Determination. The diffusion coefficients of both 2,6-AQDS and 2-AQMS were determined via two methods, first via the use of the Randles−Ševčík equation for peak current of a reversible electron transfer at a macroelectrode and second via use of a microelectrode and calculation of the diffusion coefficient from the limiting current. Solutions containing 0.1 M NaOH, 0.1 M KCl, and either 1 mM 2,6-AQDS or 2-AQMS were prepared (pH 12.6). Cyclic voltammetry was run on a gold macroelectrode from −0.4 to −0.75 V (vs SCE) at varying scan rates from 50 to 500 mV s^{-1} (results not shown). The reductive peak current was plotted against the square root of the scan rate, through use of the Randles−Ševčík equation for a reversible n electron process (eq 2);[26] it was possible to estimate the *apparent* diffusion coefficients for 2,6-AQDS and 2-AQMS as being 1.95×10^{-6} and 2.91×10^{-6} cm^2 s^{-1}.

$$i_p = (2.69 \times 10^5) n^{1.5} A C_0 D_0^{0.5} \nu^{0.5} \quad (2)$$

Here, i_p is the peak current (A), n is the total number of electrons transferred, A is the area of the electrode (cm^2), C_0 is the bulk concentration of the analyte (mol cm^{-3}), D_0 is the diffusion coefficient (cm^2 s^{-1}), and ν is the scan rate (V s^{-1}). Note these diffusion coefficients are discussed below and the true values found to be quite different in the light of microelectrode experiments, though the inapplicability of eq 2 to the process is of interest.

The size of the gold microdisk electrode was characterized via electrochemical methods. A solution containing 2 mM ferrocene and 0.1 M tetra-*n*-butylammonium perchlorate in acetonitrile was prepared. Through performing chronoamperometry and using the equation developed by Shoup and Szabo,[27] the radius of the electrode was accurately determined (not shown). This electrode was then scanned at 5 mV s^{-1} in the above pH 12.6 solutions and the limiting current for each species measured (not shown). Equation 3 describes the steady-state current at a microdisk electrode.[26] This was used to determine the diffusion coefficient; values of 5.18×10^{-6} and 4.74×10^{-6} cm^2 s^{-1} were found for 2,6-AQDS and 2-AQMS.

$$i_{ss} = 4nFD_0C_0r_0 \quad (3)$$

The notation used is the same as above, but here, i_{ss} is the steady-state current (A) at the microelectrode, F is the Faraday constant, and r_0 is the radius of the electrode (cm). There is a large discrepancy between the two methods outlined above (via use of a microelectrode or macroelectrode) for measuring the diffusion coefficients. The Randles−Ševčík equation for a multielectron transfer is based upon the assumption that the electron transfer rate is high and that the second electron transfer is sufficiently driven, so as the two redox processes occur concurrently. These assumptions do not hold for the case in question; as such, as will be shown below through a simple modeling experiment, the use of the Randles−Ševčík equation underestimates the values of D_0. In particular, the close but not connected values of the redox potentials for the first and second electron transfer lead to the cyclic voltammetry, showing a diffusional process but not one which is quantitatively consistent with eq 2. The measurement of the diffusion coefficients via the use of the microdisk are more accurate, with it not being affected by the associated electron transfer kinetics or separation between two redox potentials, since a true limiting current is measured rather than a peak current. Accordingly, the limiting current is controlled by the diffusion of AQ and at sufficiently negative potentials is a full two-electron process.

The Variation of the Voltammetric Response with pH and Ionic Strength. The electrochemical response of 2,6-AQDS and 2-AQMS was examined over the full pH range, as shown in Figure 3a and c. For both species, 1 mM solutions were prepared in buffered media and cyclic voltammetry was run in a reductive direction from an upper potential of 0.2 to −0.9 V (vs SCE) at a scan rate of 100 mV s^{-1}. As can be clearly seen from the plots, appropriate potential limits were chosen for each pH. It was not possible to measure the voltammetry of 2-AQMS below pH 1, due to the low solubility of the species in this medium.

The effect of cation concentration was studied at pH 1.1, 7, and 12.6. This was achieved through the preparation of two stock solutions. Both contained an anthraquinone derivative of 1 mM (either 2-AQDS or 2-AQMS) and the appropriate buffer; the solutions differed through one having no added KCl and the other containing 1 M KCl. From these two stock solutions, solutions with various intermediate concentrations of KCl could easily be obtained; cyclic voltammetry was run in a reductive direction on a gold macroelectrode at a scan rate of 100 mV s^{-1}. The effect of varying the KCl concentration at pH 7 and 12.6 for 2,6-AQDS is shown in Figure 4. As can be seen for these two examples, the increase in potassium concentration causes the forward peak to shift to more positive potential. Table 1 compares the effect of varying the potassium concentration on forward peak position for both anthraquinone derivatives. The above experiment was repeated with NaCl and, at pH 7, with tetra-*n*-butylammonium chloride (TBAC); all exhibited similar shifts in forward peak potential.

Modeling. Simulations were carried out using the commercial software package DIGISIM (version 3.0, BASi Technicol, West Lafayette, IN). A simple two-electron redox system involving no homogeneous reactions was set up, with the aim to identify the dependence of the peak current upon the separation in potential between the two electron transfers. All diffusion coefficients were set as 1×10^{-5} cm^2 s^{-1}, with α values of 0.5, and electron transfer rates were set at 10 cm s^{-1}, representing a likely upper value for fast electron transfer. The simulation data was then analyzed using the reversible Randles−Ševčík equation (eq 2), to obtain an apparent diffusion coefficient, the results for which are shown in Table 2. As can be clearly seen, in all three cases, the use of the Randles−Ševčík equation underestimated the diffusion coefficient by up to 50%, depending on the relative values of standard potentials.

For both 2,6-AQDS and 2-AQMS, three of the pK_a values within the scheme have been reported by a number of groups; Gamage et al.[18] provides a table of known values. Table 3 gives

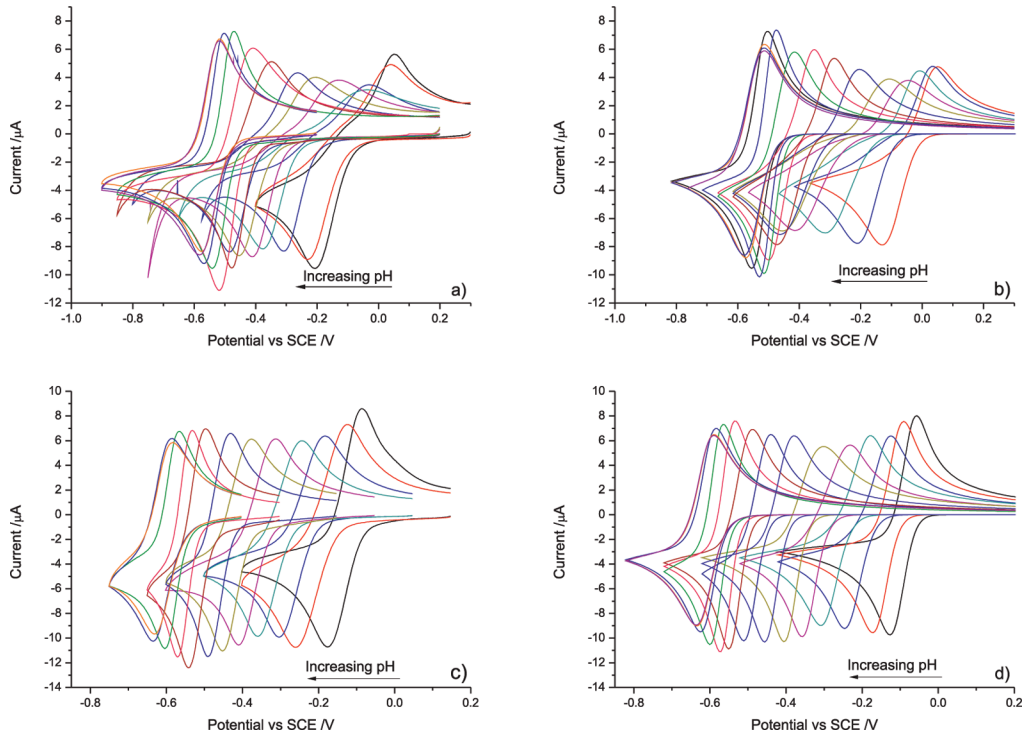

Figure 3. Overlaid cyclic voltammetry for 1 mM 2,6-AQDS (a + b) and 1 mM 2-AQMS (c + d), over the full pH range 1−13; experimental (a + c) and simulated (b + d) results are plotted separately.

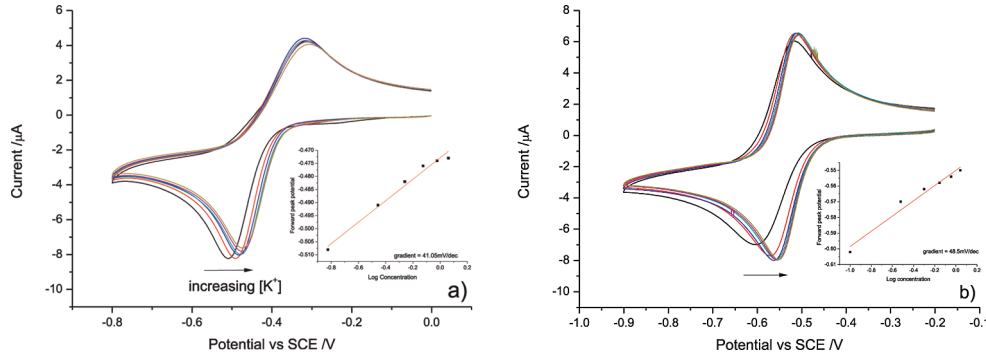

Figure 4. Overlaid cyclic voltammetry of 1 mM 2,6-AQDS at (a) pH 7 and (b) pH 12.6. The plots show the effect of addition of extra KCl to the electrolyte from 0−1 M. The insets show the plot of log cation concentration against forward peak potential.

TABLE 1: Comparison of the Forward Peak Shift with log Potassium Concentration (dec) for Both 2,6-AQDS and 2-AQMS

pH	2,6-AQDS (mV/dec)	2-AQMS (mV/dec)
1.1	12	11
7	41	12
12.6	49	14

TABLE 2: Simulated Data, for a Simple EE Process, Showing the Comparison of the Effect of Changing the Relative Redox Potentials, upon the Apparent Measured Diffusion Coefficient, Obtained from Use of the Reversible Randles−Ševčík Equation[a]

$E_1 - E_2$ (mV)	+30	0	−30
$(i_p/\nu^{0.5})$ [A(V s)$^{-0.5}$]	3.9×10^{-5}	4.3×10^{-5}	4.7×10^{-5}
calculated D_0 (cm s^{-1})	5.2×10^{-6}	6.5×10^{-6}	7.6×10^{-5}

[a] The actual diffusion coefficient used within the simulation is 1×10^{-5} cm^2 s^{-1}.

the values used within this work taken from the literature for simulation purposes; note the pK_a value used for the 2-AQMS semiquinone is marginally higher than the given literature values due to improved simulation results. All protonations were assumed to be fully buffered; consequently, the following equilibrium can be used within DIGISIM:

$$\mathrm{B} \rightleftharpoons \mathrm{A}$$
$$K_{eq} = \frac{K_a}{[H^+]}$$

Here, A is the unprotonated form, B the protonated form, and K_a is the actual acid dissociation constant for the species B.

Realistic rate constants must be used within the simulation; as such, the rate constant for protonation must and can be no larger than 1×10^{10} dm^3 mol^{-1} s^{-1} (diffusion limited). It can also be shown that, with the equilibrium used above, the rate constant for protonation should be dependent upon the proton concentration. Within the model, all diffusion coefficients were set as equal and values taken were those measured from the steady-state current at a microdisk electrode; see comment for explanation. Further, all electron transfer coefficients, α, were set as 0.5.

TABLE 3: pK_a Values Used within This Work[a]

	2,6-AQDS	2-AQMS
pK_a 1	0	0.84
pK_a 2	3.2*	4.3*
pK_a 3	10.5*	11*
pK_a 5	4.8	3.12
pK_a 6	7.6*	7.6*

[a] Values marked with an asterisk are taken from work by Gamage et al.;[18] others are calculated from optimized standard potentials used with the simulations.

TABLE 4: Values for the Standard Potentials and Electron Transfer Rates Obtained from the Optimized Simulation for Both 2,6-AQDS and 2-AQMS

redox couple	standard potential (V vs SCE)	electron transfer rate (cm s^{-1})
	2,6-AQDS	
E_1	−0.52899	0.025
E_2	−0.56499	0.1
E_3	−0.34	1
E_4	−0.13359	10
E_6	0.02919	0.0189
	2-AQMS	
E_1	−0.6061	10
E_2	−0.62101	0.38067
E_3	−0.3995	10
E_4	−0.22681	10
E_6	0.03813	10

At high pH, i.e., above pH 12, both anthraquinone derivatives should exhibit a simple EE process with no coupled homogeneous reactions (protonations), between, before, or after the electron transfer steps; this allows the values of E_1 and E_2 and the associated electron transfer rates to be obtained through fitting. As the pH is decreased, the reduction product changes from the unprotonated to the monoprotonated forms and finally to the diprotonated form as the respective pK_a's are passed. This change in equilibrium causes a Nernstian shift in the observed E_0 for the redox couple. If the simulation is limited to an EECC mechanism, then at higher proton concentrations (below about pH 6) the back-peak (oxidative wave) decreases in size, as the shift in equilibrium toward the protonated form promotes apparent irreversibility. A similar situation was found by Streeter et al.[28] where the instability of the reduced 2,6-diphenylpyrylium cation led to an apparent irreversible electrochemical response. As a consequence, to allow a description of the anthraquinone sulfonate derivative redox system at lower pH, other mechanistic pathways must be included. The issue of apparent irreversibility of the EECC mechanism is predominately solved through the inclusion of $AQH_2^{\bullet+}$, $AQH^{\bullet}$, and AQH^{+} as intermediates. If the intermediates $AQH_2^{\bullet+}$ and AQH^{+} are not included within the simulation, it is not possible to produce a system in which a good fit is obtained over the full pH range; this arises due to the ECEC mechanism becoming more irreversible in nature at higher proton concentrations. We assume that, because of the extreme difficulty of doubly protonating AQ, such that AQH_2^{2+} is an unknown species in aqueous solution (to the best of the authors' knowledge), that the e^-, H^+ sequence by which AQ is reduced to AQH_2 does not involve AQH_2^{2+} as an intermediate within the embraced pH range of this study. This model was then optimized to give a best fit; the two major fitting characteristics considered were peak position and peak current. Table 4 gives the optimized values for the potentials and electron transfer rates for the two AQ derivatives. The overlaid simulated voltammetry obtained from these values is depicted in Figure 3 for both 2,6-AQDS (b) and 2-AQMS (d). Analysis of these optimized simulations allows the dominant mechanistic pathway at varying pH to be obtained.

Discussion

The overpotential associated with the 2,6-AQDS redox system is larger than that for 2-AQMS. The sulfonate groups present have a negative charge at all pH's tested due to having a pK_a value of around −9; as a consequence, when the system undergoes a two-electron reduction, the result is a highly charged 4− ion. In alkaline medium above pH 7.6, where the formation of the mono and unprotonated forms is not negligible, there is a substantial shift in reduction potential with cation concentration, as can be seen from Table 1. Gamage et al.[17] demonstrated through X-ray crystallography that there is a likely interaction between the sulfonate and quinone oxygen groups. Interestingly, at higher pH (12.6) where the unprotonated species will be formed, the effect of the cation concentration is greater than at pH 8 where the monoprotonated form dominates; this corroborates the conclusion that it is the direct interaction between the two negatively charged groups that causes a larger overpotential for the reduction. This overpotential probably originates from a change in shape between either the quinone and semiquinone or seminquinone and hydroquinone species.[26] Due to the distance between the two oxygen groups, they are observed to be only marginally affected by the nature and size of the cation present; even with the use of TBAC, a very large and bulky cation, reduction of the overpotential occurred when added to the electrolyte.

An accurate measurement of the diffusion coefficients for both species is important for the production of a reliable simulation; as mentioned above, there is a large discrepancy between the macroelectrode and microelectrode experimental results. If the Randles−Ševčík equation is used for the analysis of systems involving the transfer of multiple electrons, in which the subsequent electron transfer steps are not sufficiently driven, there is an error when used for the analysis of the diffusion coefficients involved. This arises due to the increased probability of the intermediate species diffusing away from the electrode surface before being further oxidized or reduced, causing a decrease in the peak current. The data presented within this work serves to highlight the inadequacies of measuring the diffusion coefficient via use of the Randles−Ševčík equation, for an organic molecule involving multiple electron transfers, when the latter electron transfers are not fully driven to completion at the potentials of the first electron transfer. As an alternative, the measurement of the diffusion coefficient through analysis of the steady-state current at a microelectrode allows its accurate determination without the influence of associated electron transfer kinetics. As such, the values obtained from the microdisk experiment were used in the theoretical model.

Note that the simulation in the present case predicts the variation of peak current height (of both the forward and back waves) vs pH, as shown in Figure 5. This factor together with the voltammetric peak to peak separation and wave shape were taken to be the key features requiring simulation. Quantitative agreement was possible with the assumption of equal diffusion coefficients for all of the anthraquinone species, provided some unusual features of the system were recognized. Moreover, in the absence of this recognition, no fits were possible across the pH range. The first unusual factor is that the rapid protonation seen at low pH following electron transfer can promote the electrochemical *irreversibility* of couples, which are normally thought to show rapid electron transfer (i.e., quinone/semi-

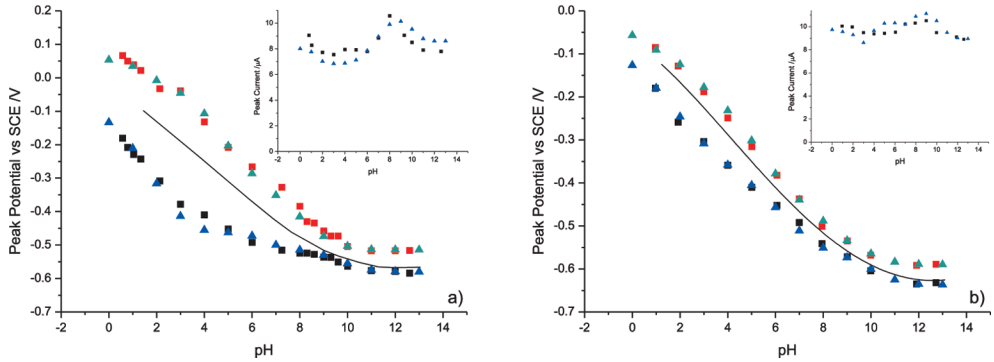

Figure 5. Comparison of experimental (exp) and simulated (sim) results for (a) 2,6-AQDS and (b) 2-AQMS. The main plots show peak potential versus pH: reductive peak, black squares (exp) and blue triangles (sim); oxidative peak, red squares (exp) and green triangles (sim). The black line represents the E_0 values as taken from work by Conant et al.[29] The insets depict the variation of peak height with pH for both the experimental (black squares) and simulated (blue triangles) results.

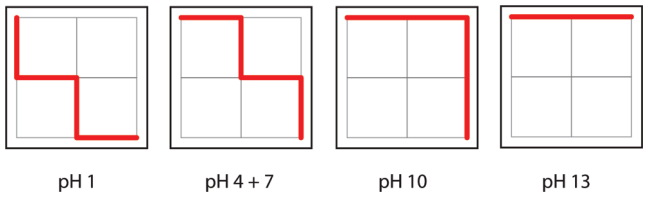

Figure 6. Scheme showing the major mechanistic pathways for both 2,6-AQDS and 2-AQMS at varying pH. Horizontal movement represents electron transfer and vertical represents proton transfer, as per Figure 2.

quinone and semiquinone/hydroquinone). This factor influences both the wave shape and the voltammetric peak to peak separation. A second unusual factor is the close similarity of the formal potentials of the two couples; this leads to the cyclic voltammetry showing diffusional characteristics but with the peak current unrelated to the unusual expressions for simple n electron reversible or irreversible behavior. Finally, the pK_a's of the quinone, semiquinone, and hydroquinone do not necessarily show comparable trends to each other, so that the model needs to consider a wide range of pK_a parameters to identify a correct fit.

As observed by Conant et al.,[29] the addition of a sulfonate group in either the 1 or 2 position adjacent to a quinone oxygen causes a shift of around +40 mV of the E_0 due to the electron withdrawing nature of the added sulfonate group. This observation is born out in practice, with the E_0 values provided by Conant et al.[29] (plotted as a black line in Figure 5) being in good agreement with the experimental results. The simulation was optimized so as to get a best fit with experiment, the primary criteria being the peak position (V) and peak height (A). Figure 5 shows the comparison between these two measurements. A good fit was obtained over the full pH range.

The model provided allows assessment of the dominating mechanistic pathway for the reduction of the two compounds at various pHs; this is achieved through selectively "switching off" pathways within the scheme. Due to the similarities in the pK_a values for the two species, at the pH's selected, the same mechanistic pathways operate for both compounds. Figure 6 gives a graphical representation of these mechanisms; here, horizontal movement indicates an electron transfer and vertical movement represents a proton transfer, as per Figure 2. It is of importance to note that, although these are the dominant pathways at each pH, other mechanistic routes may contribute to the observed current; certainly, in regions between the selected pH's, multiple routes may occur concurrently. The relative contributions to the peak current of each pathway are also not only dependent upon the equilibrium position for each protonation, but importantly for 2,6-AQDS, the relative rates of electron transfer will also have an effect. It is also of worth noting that the forward and back reaction routes may not be the same, as it is possible for the rate determining electron transfer step to change with potential.

Conclusion

For the first time, a "scheme of squares" model has been used to produce an accurate description of a $2H^+$, $2e^-$ redox system over the full pH range with direct comparison to experimentally produced cyclic voltammetry. This analysis has provided quantitative information on the pK_a's and E_0's involved within the systems and allowed the dominant mechanistic routes to be resolved at varying pH; subsequently, this greater understanding will provide a basis upon which more sensitive and sophisticated DNA hybridization sensors can be developed. The model demonstrates how the pK_a values of the anthraquinone intermediates dominate the observed voltammetry. The change in proton concentration not only causes a Nernstian shift in the measured electrochemical potential for the redox couple but also results in changes in the mechanistic pathway. At high pH, a simple EE process is found to occur, as the pH decreases the formation of other protonated species becomes possible, around pH 10 the mechanism is shown to be an EECC process, at pH 4−7 the redox process follows an ECEC route, and finally in acidic conditions (around pH 1) the mechanism is shown to likely follow a CECE process. Further, the work has highlighted the significant dependence of the redox system upon cation concentration, in certain pH ranges.

References and Notes

(1) Jacq, J. *J. Electroanal. Chem.* **1971**, *29*, 149–180.
(2) Zhang, J.; Song, S.; Wang, L.; Pan, D.; Fan, C. *Nat. Protoc.* **2007**, *2*, 2888–2895.
(3) Wang, Z.; Yang, Y.; Leng, K.; Li, J.; Zheng, F.; Shen, G.; Yu, R. *Anal. Lett.* **2008**, *41*, 24–35.
(4) Elena, D.; Oscar, R.; Arantzazu, N. *Anal. Chem.* **2004**, *76*, 3132–8.
(5) Alfonta, L.; Singh, A. K.; Willner, I. *Anal. Chem.* **2001**, *73*, 91–102.
(6) Choi, Y.-S.; Lee, K.-S.; Park, D.-H. *Curr. Appl. Phys.* **2006**, *6*, 777–780.
(7) Erdem, A.; Kerman, K.; Meric, B.; Akarca, U.; Ozsoz, M. *Anal. Chim. Acta* **2000**, *422*, 139–149.
(8) Carter, M. T.; Rodriguez, M.; Bard, A. J. *J. Am. Chem. Soc.* **1989**, *111*, 8901–8911.
(9) Wong, E.; Mearns, F.; Gooding, J. *Sens. Actuators, B* **2005**, *111*−*112*, 515–521.

(10) Kowalczyk, A.; Nowicka, A.; Jurczakowski, R.; Niedzialkowski, P.; Ossowski, T.; Stojek, Z. *Electroanalysis* **2010**, *22*, 49–59.
(11) Castano-Alvarez, M.; Fernandez-Abedul, M.; Costa-Garcia, A. *Electrophoresis* **2007**, *28*, 4679–4689.
(12) Kelley, S.; Barton, J. *Science* **1999**, *283*, 375–381.
(13) Kelley, S.; Boon, E.; Barton, J.; Jackson, N.; Hill, M. *Nucleic Acids Res.* **1999**, *27*, 4830–4837.
(14) Wong, E.; Gooding, J. *Anal. Chem.* **2003**, *75*, 3845–3852.
(15) Wong, E.; Gooding, J. *Aust. J. Chem.* **2005**, *58*, 280–287.
(16) Zhong, C.; Hu, Q. *J. Pharm. Sci.* **2003**, *92*, 2284–2294.
(17) Gamage, R.; Peake, B.; Simpson, J. *Aust. J. Chem.* **1993**, *46*, 1595–1604.
(18) Gamage, R.; McQuillan, A.; Peake, B. *J. Chem. Soc., Faraday Trans.* **1991**, *87*, 3653–3660.
(19) Laviron, E. *J. Electroanal. Chem.* **1983**, *146*, 15–36.
(20) Laviron, E. *J. Electroanal. Chem.* **1984**, *164*, 213–227.
(21) Rosso, K.; Smith, D.; Wang, Z.; Ainsworth, C.; Fredrickson, J. *J. Phys. Chem. A* **2004**, *108*, 3292–3303.
(22) Quan, M.; Sanchez, D.; Wasylkiw, M.; Smith, D. *J. Am. Chem. Soc.* **2007**, *129*, 12847–12856.
(23) Malinowski, E.; Barber, M.; Whitaker, G.; Smith, E. *J. Chemom.* **2007**, *21*, 520–528.
(24) Smith, E.; Davis, C.; Barber, M. *Anal. Biochem.* **2003**, *323*, 114–121.
(25) Henstridge, M. C.; Wildgoose, G. G.; Compton, R. G. *Langmuir* **2010**, *26*, 1340–1346.
(26) Compton, R. G.; Banks, C. E. *Understanding Voltammetry*; World Scientific Publishing: Singapore, 2007.
(27) Shoup, D.; Szabo, A. *J. Electroanal. Chem.* **1982**, *140*, 237–245.
(28) Streeter, I.; Jenkinson, S.; Fleet, G.; Compton, R. *J. Electroanal. Chem.* **2007**, *600*, 285–293.
(29) Conant, T.; Kahn, H.; Fieser, L.; Kurtz Jr., S. *J. Am. Chem. Soc.* **1922**, *44*, 1383–1396.

JP1008187